Electrostatic Nonlinear Dispersive Parametric Mode Interaction

Xiaopeng Sun
National University of Defense Technology
Xin Zhou (zhouxin11@nudt.edu.cn)
National University of Defense Technology https://orcid.org/0000-0002-7726-7809
Xingjing Ren
National University of Defense Technology
Lan Li
National University of Defense Technology
Tongqiao Miao
National University of Defense Technology
Kuo Lu
National University of Defense Technology
Xuezhong Wu
National University of Defense Technology
Dingbang Xiao
National University of Defense Technology

Research Article

Keywords: MEMS resonator, Modal coupling, Electrostatic nonlinearity, Multiple-time-scale method, Dispersive parametric coupling

Posted Date: April 25th, 2022

DOI: https://doi.org/10.21203/rs.3.rs-1512857/v1

Electrostatic Nonlinear Dispersive Parametric Mode Interaction

Xiaopeng Sun, Xin Zhou*, Xingjing Ren, Lan Li, Tongqiao Miao, Kuo Lu, Xuezhong Wu and Dingbang Xiao

College of Intelligence Science and Technology, National University of Defense Technology, Changsha 410073, China, zhouxin11@nudt.edu.cn

*Correspondence: zhouxin11@nudt.edu.cn (X.Z.)

Abstract: Understanding and controlling the nonlinear coupling in micro/nanomechanical resonators are of great importance to the exploitation of advanced devices. The recently observed electrostatic nonlinear parametric coupling is a very interesting topic. However, the theoretical model of the electrostatic parametric coupling still remains unclear. This paper explicitly derives the model and the electrostatically induced dispersive parametric coupling which reveals the ability of tuning the bifurcation topology of capacitive resonators is analyzed based on the multiple-time-scale method. A novel displacement-to-frequency transduction scheme based on this electrostatic dispersive parametric coupling effect is proposed. The transduction sensitivity is theoretically given, which indicates that this electrostatic dispersive transduction scheme can provide even more design freedoms than the existing displacement-to-frequency transduction scheme based on tension modulation. In addition, a bifurcation reversal effect is predicted in the strong actuated states of the dispersive parametric coupled system, which reveals the ability of tuning the bifurcation topology of capacitive resonators.

Keywords: *MEMS resonator, Modal coupling, Electrostatic nonlinearity, Multiple-time-scale method, Dispersive parametric coupling*

1. Introduction

Micro- and nanomechanical resonators are widely used as the cores of timing [1,2], sensing [3–5], information processing [6,7], and quantum experiments [8,9], because of their abundant mechanisms of coupling with various physical fields. The mutual inter-actions between different degrees of freedom in micro and nanomechanical resonators have attracted great attention in recent years. Understanding and efficiently manipulating modal coupling effects are very important for developing novel devices and improving performance of the existing devices [7,9–12]. Modal coupling effects exist in many different mechanisms, such as mechanical linkages, dielectric coupling, tension-induced parametric coupling, internal resonance, electrostatic coupling and so on [13–19]. Modal interactions induced by nonlinear effects are of special interest, which take tension-induced parametric coupling as the typical representative [20,21]. Among the vibrating mechanical resonators with tension generated, the displacement of one mode can affect the others' dynamics resulting from the stiffness hardening characteristic. The couplings usually consist of dispersive parametric coupling and dissipative parametric coupling, which corresponds to the affected resonant frequency and damping ratio, respectively.

The dispersive parametric coupling caused by displacement-induced tension in resonators with clamped-clamped topology has been extensively studied. Ref. [13] demonstrated that the displacement-induced tension coupling in a doubly-clamped beam resonator can detect the displacement of any other mode by measuring the response of one mode. Ref. [15] engineered a strain-coupled nanomechanical beam with a high degree of linearity between the frequency shift of the coupled modes. Ref. [18] revealed the emergence of both dispersive parametric coupling and dissipative parametric coupling in a micromechanical resonator embedded with a nanomechanical resonator. Ref. [23] realized mechanically induced transparency and mode cooling in a phonon cavity on account of strain-induced parametric coupling with a sufficient rate, simulated by solving the coupled-Van der Pol−Duffing equations numerically based on rotating frame approximation. Ref. [24] analyzed the bifurcation near the fixed points and derived the threshold of vibration coupling between the second and third modes of

an electrically actuated clamped–clamped microbeam caused by geometric nonlinearity. Though the aforementioned tension-induced parametric coupling is usually limited to clamped–clamped or thin film resonators and always negligible for most centrally anchored or bulk-fabrication-process resonators, they can provide great enlightenment for the research of other kinds of modal coupling.

With the well-known stiffness-softening characteristic, electrostatic nonlinearity often occurs in most capacitive micromechanical resonators. Due to the existence of shared capacitance in these devices, the response of any mode (oscillator) can affect the electric potential energy of the whole system, so different modes (oscillators) might interact with each other. Recently, electrostatic-nonlinearity induced parametric modal coupling effect in a capacitive microelectromechanical ring resonator was observed [19], which also showed that the mode coupling strength can be dynamically tuned with great flexibility in the control of the coupling stiffness. This kind of nonlinear parametric coupling is regarded as a very efficient coupling and does not have topology restriction of the resonator, which is even more widespread than the tension-induced one. The following-up researches indicate that the same coupling can also be found on other kinds of capacitive resonators [25,26]. They analyzed the direction and range of the frequency shift as well as the location of the frequency hopscotch in the employed tuning fork resonator. Though the experimental results are substantial, the detailed theoretical model, more precise physical pictures, and potential intriguing applications are yet to be given for this electrostatic-induced nonlinear parametric modal coupling.

In this paper, we provide the thorough theoretical model for the electrostatic-nonlinearity induced parametric modal coupling effect. The explicit expressions of the frequency responses of the coupled modes are given. Numerical analyses based on those expressions are provided as well. The electrostatically-induced dispersive parametric coupling effect are perfectly simulated numerically. A novel displacement-to-frequency transduction scheme based on this electrostatic dispersive parametric coupling effect is proposed, and the transduction sensitivity is given theoretically. The ability of electrostatic dispersive parametric coupling to tune the bifurcation topology of capacitive resonators is shown by demonstrating a bifurcation reversal effect. This paper is organized as follows. In Section 2, the theoretical model for the electrostatic nonlinear coupling is developed, which is then solved based on the multiple time scale analysis. In Section 3, the electrostatic nonlinear coupling effect is analyzed based on the theoretical model, and a novel electrostatic dispersive parametric transduction scheme is proposed. A bifurcation reversal effect is predicted as well. Finally, this work is ended with a conclusion and outlook in Section 4.

2. Theoretical Model for Electrostatic Nonlinear Parametric Coupling

2.1. Coupling Model

To introduce the electrostatic nonlinear parametric coupling that occurs in capacitive micro-electro-mechanical resonators, we consider models depicted in Figure 1. Figure 1(a) shows two mechanical oscillators sharing a common capacitor biased with a constant voltage V_0. The two oscillators can represent two distinct mechanical resonators [27], or two individual normal modes in a common resonator [19]. For the latter case, the modulation of the capacitive distance is equal to the superposition of the displacements of the two normal modes. In Figure 1(b), a flexible electrically-charged micro/nano-scale rod, beam, or wire resonator [28–30] is placed near an oppositely-charged rigid base electrode. The charge on the resonator is approximately constant q. The superposed displacements of different normal modes in the resonator modulate the capacitive distance.

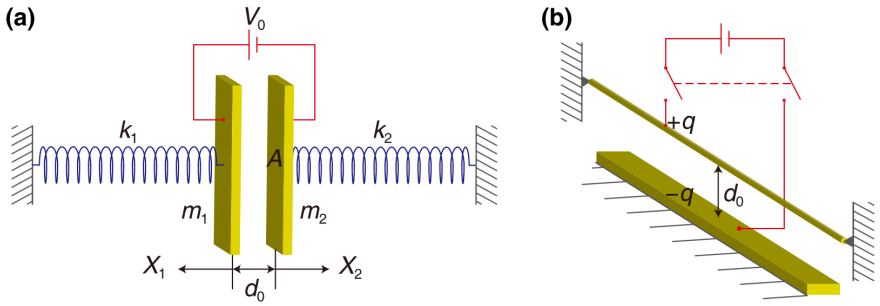

Fig. 1 Schematic of the micro/nano-mechanical systems that exhibit electrostatic nonlinear parametric coupling. (**a**) Two oscillators sharing a common capacitor biased with a constant voltage V_0. The displacements of both oscillators will affect the capacitive distance and the direction of the arrow just indicates the positive direction we artificially specify. (**b**) Flexible electrically-charged micro/nano-scale rod, beam, or wire resonator near an oppositely-charged rigid base electrode. The superposed displacements of different normal modes in the resonator modulate the capacitive distance.

Here, we consider a two-modes system. The effective stiffness and mass of each mode are represented by k_j and m_j, where j = 1, 2 indicates the mode label. d_0 is the capacitive distance at equilibrium when the capacitor is not charged. X_j indicates the effective displacement of the mode j. For the systems that the biased voltage is kept constant in Figure 1(a), the additional electrostatic potential energy is given by [19]

$$-\frac{A\epsilon_0 V_0^2}{2(d_0+X_1+X_2)}, \tag{1}$$

where A is the effective area of the common capacitor, ϵ_0 is the permittivity of the vacuum. We suppose the resonators are characterized at high vacuum environment. For the systems that the charge is kept constant in Figure 1(b), the electrostatic potential energy is given by [31]

$$-\frac{\kappa q^2}{4\pi\epsilon_0(d_0+X_1+X_2)}, \tag{2}$$

where κ is a numerical factor of order unity that is related to the dimensions and shapes of the resonator and electrode. Here, we can just express the electrostatic potential energy in a general form

$$-\frac{C}{d_0+X_1+X_2}, \tag{3}$$

where the factor C is given by $A\epsilon_0 V_0^2/2$ for the constantly biased case or $\kappa q^2/4\pi\epsilon_0$ for the constantly charged case.

The Lagrangian of the coupled-two-modes system is given by

$$L=\frac{1}{2}m_1\dot{X}_1^2+\frac{1}{2}m_2\dot{X}_2^2-\frac{1}{2}k_1X_1^2-\frac{1}{2}k_2X_2^2+\frac{C}{d_0+X_1+X_2}=0. \tag{4}$$

Substituting into the Lagrange's equation, we obtain the dynamical equations of motion,

$$m_1\ddot{X}_1+k_1X_1+\frac{C}{(d_0+X_1+X_2)^2}=0, \tag{5}$$

$$m_1\ddot{X}_2+k_2X_2+\frac{C}{(d_0+X_1+X_2)^2}=0. \tag{6}$$

When the electric voltage or charge are applied, a steady electrostatic force will cause an offset for the equilibrium position of the resonator. The new equilibrium positions X_j^* of the two modes are given by

$$k_1X_1^*=k_2X_2^*=-\frac{C}{(d_0+X_1^*+X_2^*)^2}. \tag{7}$$

We define the new displacements from the new equilibrium positions $x_j = X_j - X_j^*$ and denote the capacitive distance at new equilibrium $d_1 = d_0 + X_1^* + X_2^*$. The nonlinear electrostatic restoring forces in (5) and (6) can be expanded into the Taylor series with respect to X_1 and X_2 at the new-equilibrium positions. By introducing damping and actuation terms, the equations of motion are further given by

$$\ddot{x}_1 + \gamma_1\dot{x}_1 + \omega_1^2 x_1 - \frac{2C}{m_1 d_1^3}x_2 + \frac{3C}{m_1 d_1^4}(x_1+x_2)^2 - \frac{4C}{m_1 d_1^5}(x_1+x_2)^3 = \frac{F_1}{m_1}\cos(\omega_{d1}t), \tag{8}$$

$$\ddot{x}_2 + \gamma_2\dot{x}_2 + \omega_2^2 x_2 - \frac{2C}{m_2 d_1^3}x_1 + \frac{3C}{m_2 d_1^4}(x_1+x_2)^2 - \frac{4C}{m_2 d_1^5}(x_1+x_2)^3 = \frac{F_2}{m_2}\cos(\omega_{d2}t), \tag{9}$$

where $\omega_j = (k_j - 2C/m_j d_1^3)^{1/2}$ indicates the angular resonant frequency considering the electrostatic-negative-stiffness effect, γ_j represents the damping rate of mode j. F_j and ω_{dj} are the amplitude and angular frequency of the external force independently applied upon mode j. ω_{dj} is very close to ω_j. The above equations of motion with nonlinear coupling terms can fully describe the parametric coupling.

2.2 Multiple Time Scale Analysis

We solve those equations using multiple time scale method [32]. First, we define dimensionless variables $T=\omega_1 t^*$, $u=x_1/d_0$, $v=x_2/d_0$. a dimensionless small parameter ϵ is introduced additionally. Most applicable micro or nano resonators usually possess high quality factors ($Q = \omega_1/\gamma_1$) to obtain better performance. $Q >> 1$ holds for most of the cases. Thus, we can define $\epsilon = 1/Q = \gamma_1/\omega_1$. The equations of motion (8) and (9) are nondimensionalized as

$$D^2u + \epsilon^2\eta_1 Du + u + \epsilon^2\alpha_1 v + \epsilon\beta_1(u+v)^2 + \epsilon^2 v_1(u+v)^3 = \epsilon^2 f_1\cos(\Omega_{d1}T), \tag{10}$$

$$D^2v + \epsilon^2\eta_2 Dv + \Omega_2^2 v + \epsilon^2\alpha_2 u + \epsilon\beta_2(u+v)^2 + \epsilon^2 v_2(u+v)^3 = \epsilon^2 f_2\cos(\Omega_{d2}T), \tag{11}$$

where $D = \mathrm{d}/\mathrm{d}T$ and $D^2 = \mathrm{d}^2/\mathrm{d}T^2$ denote the differentiation operators, $\Omega_2 = \omega_2/\omega_1$, $\Omega_{d1} = \omega_{d1}/\omega_1$, $\Omega_{d2} = \omega_{d2}/\omega_1$, $\eta_1 = \omega_1/\gamma_1$, $\eta_2 = \gamma_2\omega_1/\gamma_1^2$, $\alpha_1 = -2C/m_1 d_1^3\gamma_1^2$, $\alpha_2 = -2C/m_2 d_1^3\gamma_1^2$, $\beta_1 = 3Cd_0/m_1 d_1^4\omega_1\gamma_1$, $\beta_2 = 3Cd_0/m_2 d_1^4\omega_1\gamma_1$, $v_1 = -4Cd_0^2/m_1 d_1^5\gamma_1^2$, $v_2 = -4Cd_0^2/m_2 d_1^5\gamma_1^2$, $f_1 = F_1/m_1 d_0\gamma_1^2$, $f_2 = F_2/m_2 d_0\gamma_1^2$.

Then, we define multiple time scales $T_0 = T$, $T_1 = \epsilon T$, $T_2 = \epsilon^2 T$, ⋯. The solutions of the equations (10) and (11) can be expressed in the forms

$$u = u_0(T_0,T_1,T_2) + \epsilon u_1(T_0,T_1,T_2) + \epsilon^2 u_2(T_0,T_1,T_2), \tag{12}$$

$$v = v_0(T_0,T_1,T_2) + \epsilon v_1(T_0,T_1,T_2) + \epsilon^2 v_2(T_0,T_1,T_2). \tag{13}$$

Based on the Chain Rule, we have $D = D_0 + \epsilon D_1$, $D_2 = D_0^2 + 2\epsilon D_0 D_1 + \epsilon^2(2D_0 D_2 + D_1^2)$. The higher order terms about ϵ have been neglected. D_m^n (m = 0, 1, 2, n = 1, 2) denotes the n-th order differentiation operators with respect to T_m. Substituting (12) and (13) into (10) and (11), and then equating the coefficients of the like powers of ϵ on both sides, we obtain

Order ϵ^0

$$D_0^2 u_0 + u_0 = 0, \tag{14}$$

$$D_0^2 v_0 + \Omega_2^2 v_0 = 0. \tag{15}$$

Order ϵ^1

$$D_0^2 u_1 + u_1 + 2D_0 D_1 u_0 + \beta_1(u_0+v_0)^2 = 0, \tag{16}$$

$$D_0^2 v_1 + \Omega_2^2 v_1 + 2D_0 D_1 v_0 + \beta_2(u_0+v_0)^2 = 0. \tag{17}$$

Order ϵ^2

$$\begin{aligned} &D_0^2 u_2 + u_2 + 2D_0 D_1 u_1 + (2D_0 D_2 + D_1^2)u_0 + \eta_1 D_0 u_0 + \alpha_1 v_0 \\ &+2\beta_1(u_0+v_0)(u_1+v_1) + v_1(u_0+v_0)^3 = f_1\cos(\Omega_{d1}t), \end{aligned} \tag{18}$$

$$D_0^2 v_2 + \Omega_2^2 v_2 + 2D_0 D_1 v_1 + \left(2D_0 D_2 + D_1^2\right) v_0 + \eta_2 D_0 v_0 + \alpha_2 u_0$$
$$+ 2\beta_2 \left(u_0 + v_0\right)\left(u_1 + v_1\right) + v_2 \left(u_0 + v_0\right)^3 = f_2 \cos\left(\Omega_{d2} t\right). \tag{19}$$

The general solutions of (14) and (15) can be written in the form

$$u_0 = M\left(T_1, T_2\right)\exp\left(iT_0\right) + \bar{M}\left(T_1, T_2\right)\exp\left(-iT_0\right), \tag{20}$$

$$v_0 = N\left(T_1, T_2\right)\exp\left(i\Omega_2 T_0\right) + \bar{N}\left(T_1, T_2\right)\exp\left(-i\Omega_2 T_0\right), \tag{21}$$

where $M, N \in \mathbb{C}$. The bar indicates the complex conjugation. Substituting (20) and (21) into (16) and (17) leads to

$$\begin{aligned} D_0^2 u_1 + u_1 &= -2iD_1 M \exp\left(iT_0\right) - \beta_1 M^2 \exp\left(2iT_0\right) - \beta_1 N^2 \exp\left(2i\Omega_2 T_0\right) \\ &= -2\beta_1 MN \exp\left[i\left(1+\Omega_2\right)T_0\right] - 2\beta_1 M\bar{N} \exp\left[i\left(1-\Omega_2\right)T_0\right] \\ &= -2\beta_1 |M|^2 - 2\beta_1 |N|^2 + \text{c.c.}, \end{aligned} \tag{22}$$

$$\begin{aligned} D_0^2 v_1 + \Omega_2^2 v_1 &= -2i\Omega_2 D_1 N \exp\left(i\Omega_2 T_0\right) - \beta_2 M^2 \exp\left(2iT_0\right) - \beta_2 N^2 \exp\left(2i\Omega_2 T_0\right) \\ &= -2\beta_2 MN \exp\left[i\left(1+\Omega_2\right)T_0\right] - 2\beta_2 M\bar{N} \exp\left[i\left(1-\Omega_2\right)T_0\right] \\ &= -2\beta_2 |M|^2 - 2\beta_2 |N|^2 + \text{c.c.}, \end{aligned} \tag{23}$$

where c.c. denotes the complex conjugation of the terms in front. Suppose $1 + \Omega_2$ and $1 - \Omega_2$ are far from both 1 and Ω_2, so they will not contribute the secular terms. Elimination the secular terms of (22) and (23) yields

$$-2iD_1 M = 0, \tag{24}$$

$$-2i\Omega_2 D_1 N = 0, \tag{25}$$

which means that M and N are functions of only T_2. We can further obtain the particular solutions of u_1 and v_1 from (22) and (23) after the secular terms have been eliminated. We substitute the particular solutions of u_1 and v_1 and the general solutions (20) and (21) into (18) and (19), and eliminate the secular terms gives

$$-2iD_2 M - D_1^2 M - i\eta_1 M - 2\beta_1^2 \left(\frac{2MN\bar{N}}{\Omega_2^2 - 2\Omega_2} + \frac{2MN\bar{N}}{\Omega_2^2 + 2\Omega_2} + \frac{M^2\bar{M}}{3}\right)$$
$$-2\beta_1\beta_2 \left(\frac{M^2\bar{M}}{4-\Omega_2^2} + \frac{2MN\bar{N}}{1-2\Omega_2} + \frac{2MN\bar{N}}{1+2\Omega_2}\right) - v_1\left(3M^2\bar{M} + 6MN\bar{N}\right) + \frac{f_1}{2}\exp\left(i\sigma_1 T_1\right) = 0, \tag{26}$$

$$-2i\Omega_2 D_2 N - D_1^2 N - i\eta_2\Omega_2 N - 2\beta_2^2 \left(\frac{2MN\bar{M}}{1-2\Omega_2} + \frac{2MN\bar{M}}{1+2\Omega_2} + \frac{N^2\bar{N}}{3\Omega_2^2}\right)$$
$$-2\beta_1\beta_2 \left(\frac{N^2\bar{N}}{4\Omega_2^2 - 1} + \frac{2MN\bar{M}}{\Omega_2^2 - 2\Omega_2} + \frac{2MN\bar{M}}{\Omega_2^2 + 2\Omega_2}\right) - v_2\left(3N^2\bar{N} + 6MN\bar{M}\right) + \frac{f_2}{2}\exp\left(i\sigma_2 T_1\right) = 0, \tag{27}$$

where the detuning parameters σ_1 and σ_2 are introduced according to $\Omega_{d1} = 1 + \epsilon\sigma_1$ and $\Omega_{d2} = \Omega_2 + \epsilon\sigma_2$. Based on (24) and (25), we have $D_1^2 M = 0$ and $D_1^2 N = 0$, which can be further used to simply (26) and (27).

To obtain the approximative solution, the secular conditions of the first order (24) and (25) and those of the second order (26) and (27) should hold simultaneously. We can expand those equations into the time scale of T, and combine (24) with (26) and (25) with (27), which gives

$$-2iDM - i\epsilon^2\eta_1 M - 2\epsilon^2\beta_1^2 \left(\frac{2MN\bar{N}}{\Omega_2^2 - 2\Omega_2} + \frac{2MN\bar{N}}{\Omega_2^2 + 2\Omega_2} + \frac{M^2\bar{M}}{3}\right)$$
$$-2\epsilon^2\beta_1\beta_2 \left(\frac{M^2\bar{M}}{4-\Omega_2^2} + \frac{2MN\bar{N}}{1-2\Omega_2} + \frac{2MN\bar{N}}{1+2\Omega_2}\right) - \epsilon^2 v_1\left(3M^2\bar{M} + 6MN\bar{N}\right)$$
$$+\epsilon^2 \frac{f_1}{2}\exp\left(i\epsilon\sigma_1 T\right) = 0, \tag{28}$$

$$-2i\Omega_2 DN - i\epsilon^2\eta_2\Omega_2 N - 2\epsilon^2\beta_2^2\left(\frac{2MN\bar{M}}{1-2\Omega_2}+\frac{2MN\bar{M}}{1+2\Omega_2}+\frac{N^2\bar{N}}{3\Omega_2^2}\right)$$
$$-2\epsilon^2\beta_1\beta_2\left(\frac{N^2\bar{N}}{4\Omega_2^2-1}+\frac{2MN\bar{M}}{\Omega_2^2-2\Omega_2}+\frac{2MN\bar{M}}{\Omega_2^2+2\Omega_2}\right)-\epsilon^2 v_2\left(3N^2\bar{N}+6MN\bar{M}\right)$$
$$+\epsilon^2\frac{f_2}{2}\exp\left(i\epsilon\sigma_2 T\right)=0. \tag{29}$$

We introduce polar notation to the complex amplitude of the first-order approximation

$$M=\frac{|u|}{2}\exp\left(i\varphi_1\right), \tag{30}$$

$$N=\frac{|v|}{2}\exp\left(i\varphi_2\right), \tag{31}$$

where $|u|$, $|v|$, φ_1, $\varphi_2\in\mathbb{R}$. $|u|$ and $|v|$ are the first-order approximations of the nondimensionalized amplitudes of the working modes, φ_1 and φ_2 are the first-order approximations of the nondimensionalized phases of the working modes. Substituting (30) and (31) into (28) and (29), and separating the result into real and imaginary parts, we obtain

$$\epsilon^2 f_1\sin\Phi=2\frac{\mathrm{d}|u|}{\mathrm{d}T}+\epsilon^2\eta_1|u|, \tag{32}$$

$$\epsilon^2 f_1\cos\Phi=-\frac{1}{4}\epsilon^2\Lambda_1|u|^3-\frac{1}{4}\epsilon^2\Pi_1|u||v|^2-2|u|\left(\epsilon\sigma_1-\frac{\mathrm{d}\Phi}{\mathrm{d}T}\right), \tag{33}$$

$$\epsilon^2 f_2\sin\Psi=2\Omega_2\frac{\mathrm{d}|v|}{\mathrm{d}T}+\epsilon^2\eta_2\Omega_2|v|, \tag{34}$$

$$\epsilon^2 f_2\cos\Psi=-\frac{1}{4}\epsilon^2\Lambda_2|v|^3-\frac{1}{4}\epsilon^2\Pi_2|u|^2|v|-2\Omega_2|v|\left(\epsilon\sigma_2-\frac{\mathrm{d}\Psi}{\mathrm{dT}}\right), \tag{35}$$

where $\Phi=\epsilon\sigma_1 T-\varphi_1$, $\Psi=\epsilon\sigma_2 T-\varphi_2$, and

$$\Lambda_1=-\frac{2\beta_1\beta_2}{4-\Omega_2^2}-\frac{2\beta_1^2}{3}-3v_1\approx-3v_1\approx\frac{12C}{m_1 d_0^3\gamma_1^2}, \tag{36}$$

$$\Pi_1=-\frac{4\beta_1^2}{\Omega_2^2-2\Omega_2}-\frac{4\beta_1^2}{\Omega_2^2+2\Omega_2}-\frac{4\beta_1\beta_2}{1-2\Omega_2}-\frac{4\beta_1\beta_2}{1+2\Omega_2}-6v_1\approx-6v_1\approx\frac{24C}{m_1 d_0^3\gamma_1^2}, \tag{37}$$

$$\Lambda_2=-\frac{2\beta_1\beta_2}{4\Omega_2^2-1}-\frac{2\beta_2^2}{3\Omega_2^2}-3v_2\approx-3v_2\approx\frac{12C}{m_2 d_0^3\gamma_1^2}, \tag{38}$$

$$\Pi_2=-\frac{4\beta_2^2}{1-2\Omega_2}-\frac{4\beta_2^2}{1+2\Omega_2}-\frac{4\beta_1\beta_2}{\Omega_2^2-2\Omega_2}-\frac{4\beta_1\beta_2}{\Omega_2^2+2\Omega_2}-6v_2\approx-6v_2\approx\frac{24C}{m_2 d_0^3\gamma_1^2}, \tag{39}$$

The approximations in above expressions are made based on the assumptions that $d_1\approx d_0$ and the electrostatic frequency tuning is much smaller than the resonant frequencies, $\omega_j^2\gg 2C/m_j d_3^1$, which is true in practice. We can conclude that the third-order nonlinearity coefficients are dominant in this system. The steady-state response corresponds to $\mathrm{d}|u|/\mathrm{dT}=\mathrm{d}|v|/\mathrm{dT}=\mathrm{d}\Phi/\mathrm{d}T=\mathrm{d}\Psi/\mathrm{d}T=0$, which corresponds to the solutions of

$$\epsilon^2 f_1\sin\Phi=\epsilon^2\eta_1|u|, \tag{40}$$

$$\epsilon^2 f_1\cos\Phi=-\frac{1}{4}\epsilon^2\Lambda_1|u|^3-\frac{1}{4}\epsilon^2\Pi_1|u||v|^2-2|u|\epsilon\sigma_1, \tag{41}$$

$$\epsilon^2 f_2\sin\Psi=\epsilon^2\eta_2\Omega_2|v|, \tag{42}$$

$$\epsilon^2 f_2\cos\Psi=-\frac{1}{4}\epsilon^2\Lambda_2|v|^3-\frac{1}{4}\epsilon^2\Pi_2|u|^2|v|-2\Omega_2|v|\epsilon\sigma_2. \tag{43}$$

All the frequency responses of the coupled modes are described by (40)-(43). In this paper, we only interested in the amplitude-frequency responses. Eliminating the phase variables Φ and Ψ in (40)-(43),

we obtain the amplitudes $|u|$ and $|v|$ as implicit functions of σ_1 and σ_2. Then, transforming the dimensionless parameters to the practical ones, we obtain the displacement amplitudes of the modes $|x_1|$ and $|x_2|$, which are implicitly given by

$$\frac{F_1^2}{m_1^2}-\omega_1^2\gamma_1^2|x_1|^2=\left(\frac{3C}{m_1d_0^5}|x_1|^3+\frac{6C}{m_1d_0^5}|x_1||x_2|^2+2\gamma_1\omega_1|x_1|\delta_1\right)^2, \tag{44}$$

$$\frac{F_2^2}{m_2^2}-\omega_2^2\gamma_2^2|x_2|^2=\left(\frac{3C}{m_2d_0^5}|x_2|^3+\frac{6C}{m_2d_0^5}|x_2||x_1|^2+2\gamma_1\omega_2|x_2|\delta_2\right)^2, \tag{45}$$

where $\delta_1 = \omega_{d1} - \omega_1$ and $\delta_2 = \omega_{d2} - \omega_2$ are the detuning parameters of the driving forces. The amplitude-frequency responses of the coupled nonlinear modes can be simulated by calculating $|x_1|$ and $|x_2|$ with different values of ω_{d1} and ω_{d2}. It should be noted that the results of frequency responses may contain unstable branches, which can be handled with various common methods [18,33,34]. Based on above results, the resonant frequency of one mode can be modulated by the vibration of the other mode. The frequency shifts of one mode caused by another mode can be explicitly given. We rewrite equations (44) and (45) into the forms of

$$2\gamma_1\omega_1|x_1|\delta_1=-\frac{3C}{m_1d_0^5}|x_1|^3-\frac{6C}{m_1d_0^5}|x_1||x_2|^2\pm\sqrt{\frac{F_1^2}{m_1^2}-\omega_1^2\gamma_1^2|x_1|^2}, \tag{46}$$

$$2\gamma_1\omega_2|x_2|\delta_2=-\frac{3C}{m_2d_0^5}|x_2|^2-\frac{6C}{m_2d_0^5}|x_2||x_1|^3\pm\sqrt{\frac{F_2^2}{m_2^2}-\omega_2^2\gamma_2^2|x_2|^2}. \tag{47}$$

In the square roots, the amplitudes of modes should satisfy $|x_1| \le F_1/m_1\omega_1\gamma_1$ and $|x_2| \le F_2/m_2\omega_2\gamma_2$. When both modes are at resonance, which indicates that amplitudes of both modes reach the maximum, the frequency shifts can be obtained by calculating the detunings δ_1 and δ_2 in equations (46) and (47) and applying the resonance conditions $|x_1| = F_1/m_1\omega_1\gamma_1$ and $|x_2| = F_2/m_2\omega_2\gamma_2$. The maximum frequency shift $\hat{\delta}_1$ of mode 1 caused by resonance of mode 2 and that $\hat{\delta}_2$ of mode 2 caused by resonance mode 1 are given by

$$\hat{\delta}_1=-\frac{3C}{2\gamma_1\omega_1m_1d_0^5}\left(\frac{F_1^2}{m_1^2\omega_1^2\gamma_1^2}+\frac{2F_2^2}{m_2^2\omega_2^2\gamma_2^2}\right), \tag{48}$$

$$\hat{\delta}_2=-\frac{3C}{2\gamma_1\omega_2m_2d_0^5}\left(\frac{F_2^2}{m_2^2\omega_2^2\gamma_2^2}+\frac{2F_1^2}{m_1^2\omega_1^2\gamma_1^2}\right), \tag{49}$$

respectively.

3. Dynamical Analyses of the Electrostatic Dispersive Parametric Coupling

3.1. Frequency Responses Analysis

In this Section, we analyze the electrostatic nonlinear parametric coupling in typical capacitive electromechanical systems shown in Figure 2 based on the theoretical model of (44) and (45). Figure 2(a) exhibits the schematic transient pattern of simultaneously actuated normal mode 1 and mode 2 of a resonator, a ring resonator is shown here for instance. Their displacements affect the capacitive gap in superposing form. Dispersive parametric modal interaction occurs when a nonlinear electrostatic potential is applied [19]. Figure 2(b) shows a more apparent example. Two oscillators actuated independently share a common capacitor that is biased with a constant voltage V_0 produces dispersive parametric coupling as well. During above-mentioned cases, the vibrational displacement of one mode (oscillator) can influence the resonant frequency of the other mode (oscillator).

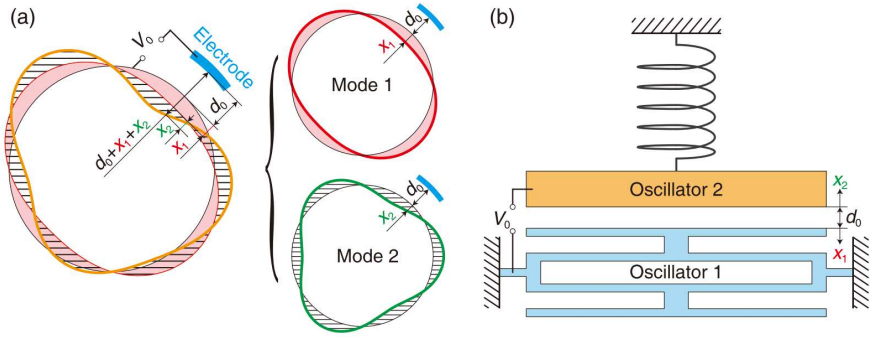

Fig.2 Typical systems that can produce electrostatic dispersive parametric coupling. (**a**) Schematic transient pattern of the simultaneously actuated modes 1 and 2 of a ring resonator [19]. (**b**) Schematic pattern of two distinct mechanical oscillators actuated independently sharing a common capacitor biased with a constant voltage. displacements of both modes (oscillators) contribute to the variation of the capacitive gap. Dispersive parametric interaction occurs when a nonlinear electrostatic potential is applied

For instance, we consider a pair of modes (oscillators) labelled by 1 and 2 with typical parameters as follows: the resonant frequencies $\omega_1 = 2\pi \times 135{,}000$ Hz and $\omega_2 = 2\pi \times 165{,}000$ Hz, the corresponding damping rates $\gamma_1 = 2\pi \times 1$ Hz and $\gamma_2 = 2\pi \times 2.5$ Hz, and modal masses $m_1 = 5.8\times10^{-9}$ kg and $m_2=4\times10^{-9}$ kg. The electrostatic factor is given by $C = A\epsilon_0 V_0^2/2$, where $V_0 = 30$ V and the capacitive area is given by $A = 5.65\times 10^{-9}$ m^2 [19].

The two modes (oscillators) are actuated simultaneously. For the case considering different modes in a single resonator (Figure 2(a)), the co-excitation of two modes can be realized by applying two driving signals. The frequency of each signal should near the resonant frequency of the corresponding mode. Each signal should be applied to electrodes located at the non-node deforming parts of the corresponding mode to guarantee actuation efficiency. For the case considering different oscillators sharing common capacitor (Figure 2(b)). The co-excitation can be easily realized by independently actuating the two oscillators. Suppose the two modes are actuated by two electrostatic forces described by

$$F_j \cos\left(\omega_{\mathrm{d}j} t\right) = \frac{A_{\mathrm{d}j}\epsilon_0}{2d_0^2}\left[V_0 + V_{dj}\cos\left(\omega_{dj} t\right)\right]^2 - \frac{A_{\mathrm{d}j}\epsilon_0}{2d_0^2}\left[V_0 - V_{dj}\cos\left(\omega_{\mathrm{d}j} t\right)\right]^2$$
$$= \frac{2A_{\mathrm{d}j}\epsilon_0 V_0 V_{\mathrm{d}j}}{d_0^2}\cos\left(\omega_{dj} t\right), \tag{50}$$

where $j = 1, 2$. $V_{\mathrm{d}j}$ is the amplitude of the alternating current driving voltage applied to mode j. $A_{\mathrm{d}j}$ is the effective area of the driving capacitive electrode of mode j. In the following analyses, we assume $A_{\mathrm{d}j} = A$ for simplicity.

If mode j is actuated while the other mode k is in free, which indicates that $F_j \neq 0$ and $F_k = 0$. There is no frequency response in mode k because $|x_k| \leq F_k/m_k\omega_k\gamma_k = 0$. While the frequency response of the mode j is given by

$$\frac{F_j^2}{m_j^2} - \omega_j^2\gamma_j^2\left|x_j\right|^2 = \left(\frac{3C}{m_j d_0^5}\left|x_j\right|^3 + 2\gamma_1\omega_j\left|x_j\right|\delta_j\right)^2, \tag{51}$$

which is the ordinary Duffing solution [32]. The amplitude-frequency responses of the solely driven modes 1 or 2 are depicted by Figure 3(a) or (b), respectively. Under the influence of the electrostatic potential, both modes show stiffness-softening Duffing responses, which just verifies the validity of the solutions obtained by the perturbation technique.

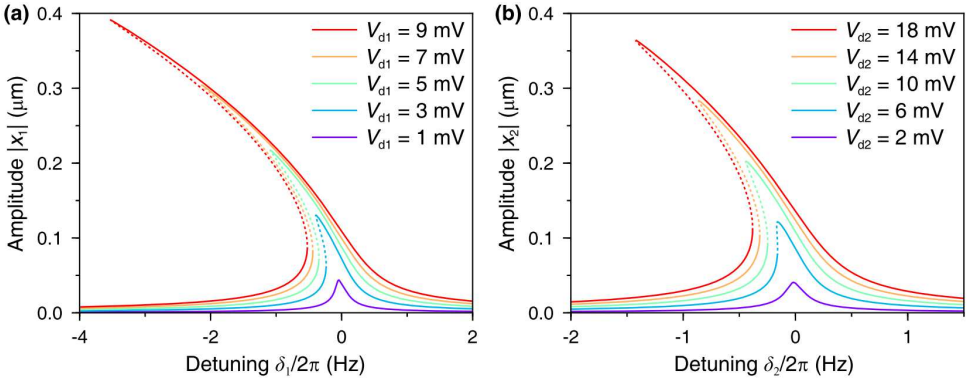

Fig.3 Amplitude-frequency responses of the solely driven (**a**) mode 1 or (**b**) mode 2 with different drive voltages simulated based on (51)

3.2. Interaction Analysis and Electrostatic Dispersive Parametric Transduction Scheme

Here, we study the simultaneously actuated cases. First, we consider the condition that both modes are weakly actuated so that both of them are not driven into the bifurcation condition [35]. Assume V_{d1} = 1 mV and V_{d2} = 3 mV, the amplitude-frequency responses of modes 1 and 2 are functions of detunings δ_1 and δ_2, as shown in Figure 4(a) and (b), which are simulated based on (44) and (45), respectively.

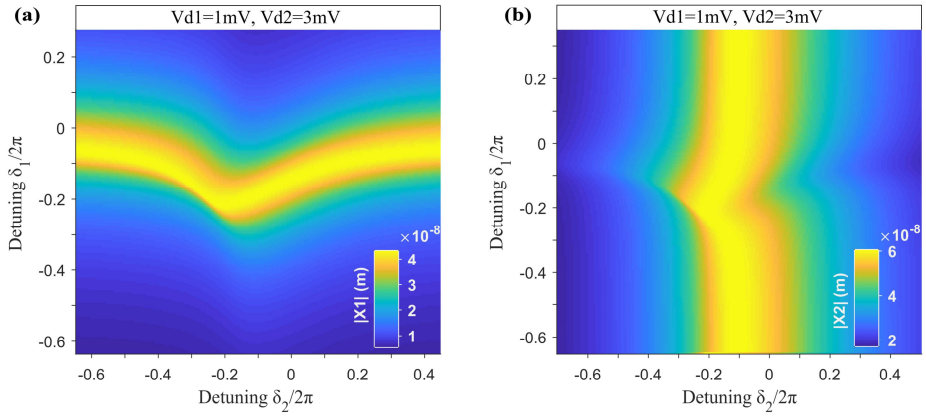

Fig.4 Simulated amplitude-frequency responses if the electrostatically coupled modes are weakly actuated. (**a**) Amplitude-frequency responses $|x_1|$ and (**b**) $|x_2|$.

It is observed that the displacement of one mode will cause a frequency dispersion to the other mode, which is very similar to the tension-induced parametric interaction found in the clamped-clamped resonator [13]. The difference is that the frequency shifts to lower values for this electrostatic nonlinear interaction, while the frequency shifts to higher values for the tension-induced nonlinear interaction [13]. In theory, this coupling is reciprocal and each one of the coupled modes can be selected to be the monitor or objective mode. But the mode with larger quality factor ($Q = \omega/\gamma$) can possess lower line width and therefore higher resolution for frequency detection, so it is more appropriate for it to be the monitor mode. In this case, mode 1 (Q_1 = 135 k) is chosen to be the monitor mode to detect the actuation intensity of the objective mode 2 (Q_2 = 66 k) by monitoring the frequency shift.

If we further increase the driving voltage of objective mode 2 to V_{d2} = 18 mV while keep that of the monitor mode 1 unchanged, V_{d1} = 1 mV. The simulated amplitude-frequency responses are shown in

Figure 5. The intensity of objective mode 2 is very clearly reflected by the resonant frequency of the monitor mode 1 shown in Figure 5 (a) and (c). Since the monitor mode 1 is weakly actuated, its back action to the objective mode 2 is relatively weaker, as shown in Figure 5 (b) and (d). These results are consistent with the experimental results in Ref. [19].

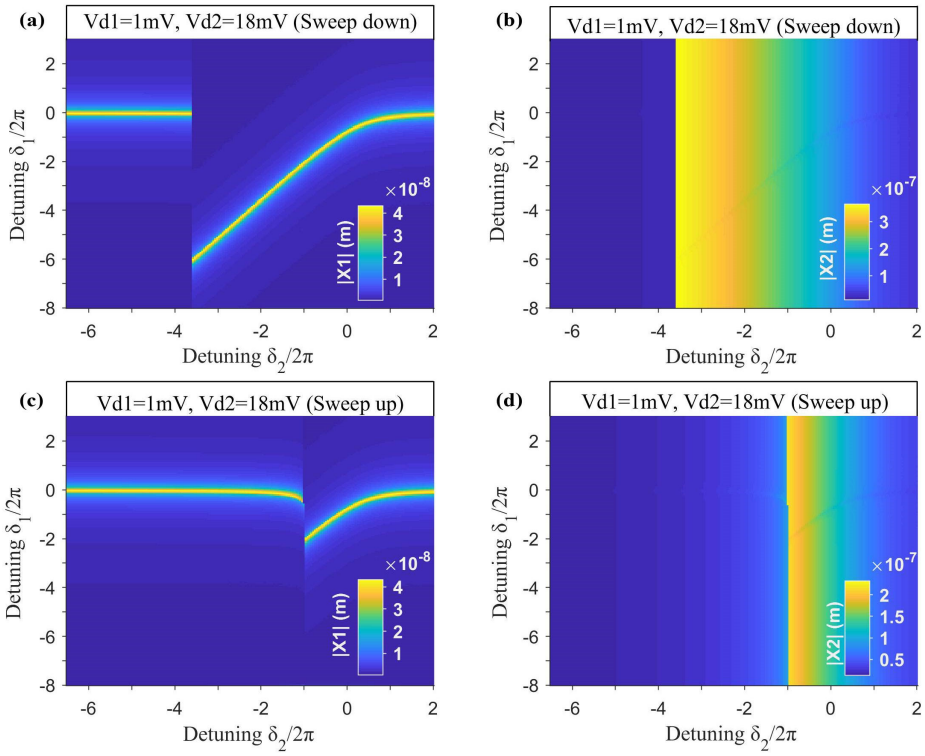

Fig.5 Simulated amplitude-frequency responses if mode 1 is weakly actuated while mode 2 is strongly actuated. (**a**) Amplitude-frequency responses $|x_1|$ and (**b**) $|x_2|$ if the driving frequency of mode 2 is changed from high to low. (**c**) and (**d**) are the results if the driving frequency of mode 2 is changed from low to high

The aforementioned analytical results concerning electrostatic modal coupling establish foundation for displacement-to-frequency transduction. The theoretical model for this detection scheme is given based on coupling model (44) and (45). Applying the resonance condition $|x_1| = F_1/m_1\omega_1\gamma_1$ to the monitor mode 1, we have

$$|x_2|^2 = -\frac{\omega_1\gamma_1 m_1 d_0^5}{3C}\delta_1 - \frac{F_1^2}{2m_1^2\omega_1^2\gamma_1^2}. \tag{52}$$

Substituting (52) into (45), we obtain frequency modulation of the monitor mode 1 (δ_1) as a function of the frequency detuning of the objective mode 2 (δ_2) given by

$$-\frac{F_2^2}{m_2^2\left(\frac{\omega_1\gamma_1 m_1 d_0^5}{3C}\delta_1 + \frac{F_1^2}{2m_1^2\omega_1^2\gamma_1^2}\right)} - \omega_2^2\gamma_2^2$$

$$= \left(-\frac{m_1\omega_1\gamma_1}{m_2}\delta_1 + \frac{9C}{2m_2 d_0^5}\frac{F_1^2}{m_1^2\omega_1^2\gamma_1^2} + 2\gamma_1\omega_2\delta_2\right)^2. \tag{53}$$

By using the weak actuation assumption of monitor mode 1 $|x_1| \ll |x_2|$, equations (52) and (53) can be further simplified to

$$\delta_1 \approx -\frac{3C}{\omega_1\gamma_1 m_1 d_0^5}|x_2|^2$$

$$\frac{F_2^2}{m_2^2}+\omega_2^2\gamma_2^2\left(\frac{\omega_1\gamma_1 m_1 d_0^5}{3C}\delta_1\right)\approx -\frac{\omega_1\gamma_1 m_1 d_0^5}{3C}\delta_1\left(-\frac{m_1\omega_1\gamma_1}{m_2}\delta_1+2\gamma_1\omega_2\delta_2\right)^2. \tag{54}$$

That the equations (54) and (55) are equivalent to the Duffing solution (51) for $j = 2$. Above analysis indicates that the frequency modulation δ_1 of the weakly driven monitor mode 1 is very good estimation of the power intensity $|x_2|^2$ of the objective mode 2. The detection sensitivity of this dispersive parametric transduction is given by

$$S=-\frac{3C}{2\pi\omega_1\gamma_1 m_1 d_0^5}, \tag{55}$$

which is calculated to be 46 Hz μm^{-2} for the current design. The variation range of the frequency modulation δ_1 of the weakly driven monitor mode 1 are given by

$$-\frac{3C}{2\omega_1\gamma_1 m_1 d_0^5}\left(\frac{F_1^2}{m_1^2\omega_1^2\gamma_1^2}+\frac{2F_2^2}{m_2^2\omega_2^2\gamma_2^2}\right)\le\delta_1\le-\frac{3C}{2\omega_1\gamma_1 m_1 d_0^5}\left(\frac{F_1^2}{m_1^2\omega_1^2\gamma_1^2}\right). \tag{56}$$

The frequency modulation δ_1 of the monitor mode 1 as function of the frequency detuning δ_2 of the objective mode 2 with different actuation voltages are depicted in Figure 6.

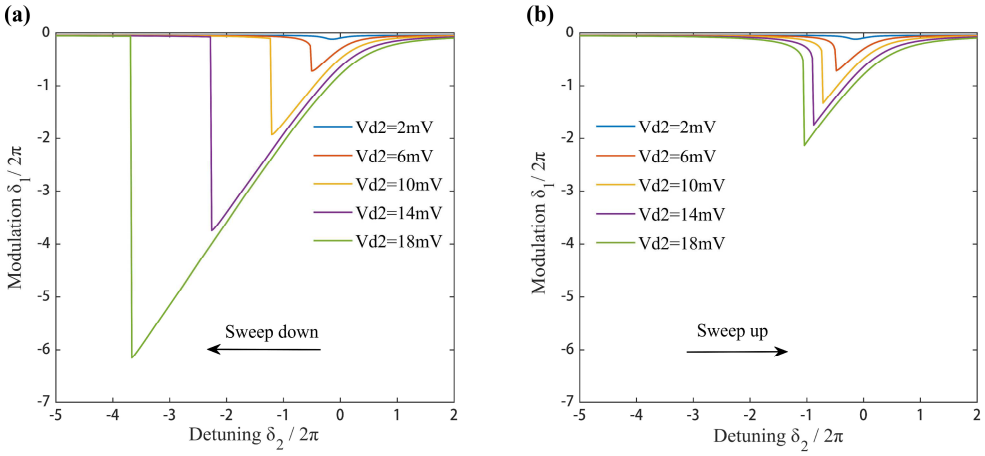

Fig. 6 Frequency modulation of the monitor mode 1 δ_1 as function of the driving frequency detuning of the objective mode 2 with different driving intensities. Simulated based on (53) (**a**) δ_1 if the detuning of mode 2 is changed from high to low and (**b**) is that from low to high

The electrostatically-induced dispersive parametric coupling can be used to engineer a displacement transducer. The key part of this transducer is a particular designed monitor oscillator that is capacitively coupled to the objective oscillator. The power intensity of the objective oscillator can be measured by detecting the frequency modulation of the monitor oscillator. The dispersive parametric transduction sensitivity S given by (56) is only related to the parameters of the monitor oscillator and the coupling capacitance, which can be designed to obtain higher sensitivity. The dispersive parametric transduction sensitivity (56) can be further expanded for the constant-voltage biased or constant-charged conditions to S_V and S_q, respectively, which are given by

$$S_V=-\frac{3A\epsilon_0 V_0^2}{4\pi\omega_1\gamma_1 m_1 d_0^5}=-\frac{3A\epsilon_0 V_0^2 Q_1}{4\pi d_0^5 k_1}, \tag{57}$$

$$S_q=-\frac{3\kappa q^2}{8\pi^2\epsilon_0\omega_1\gamma_1 m_1 d_0^5}=-\frac{3\kappa q^2 Q_1}{8\pi^2\epsilon_0 d_0^5 k_1}, \tag{58}$$

where $Q_1 = \omega_1/\gamma_1$ and $k_1 = \omega_1^2 m_1$ are the quality factor and effective stiffness of the monitor resonator, respectively.

To have a better sensitivity, the monitor resonator with higher quality factor, lower stiffness, and lower mass should be designed. The ideal design for the monitor resonator is the double-end-tuning-fork, as shown by the oscillator 1 in Figure 2(b). For the constant-voltage biased condition, the capacitive gap should be reduced, the capacitive area should be increased, and the biased voltage should be increased. For the constant-charged condition, the capacitive gap should be reduced, the factor κ should be increased by optimizing the geometry of the monitor resonator, and the charge should be increased.

3.3. Bifurcation Reversal Effect

If the two modes are strongly excited to bifurcation states simultaneously, the characteristic of the coupling changes significantly, as shown in Figure 7. First, we drive mode 1 alone with a strong driving voltage of V_{d1} = 4 mV to obtain a stiffness-softening bifurcation state, as shown by the blue curve corresponding to $V_{d2} = 0$ in Figure 7(b). If we maintain the actuation condition of mode 1, while apply a strong drive (V_{d1} = 22 mV) to mode 2 near its resonant frequency simultaneously, the amplitude-frequency response of mode 1 changes with respect to the detuning δ_2. Especially, there is a transition of bifurcation at the point $\delta_2 = 0$ from stiffness-softening type to the stiffness-hardening type. The curve ii in Figure 7(a) is depicted by the red curve in Figure 7(b), whose bifurcation is reversed compared with the original one (blue curve).

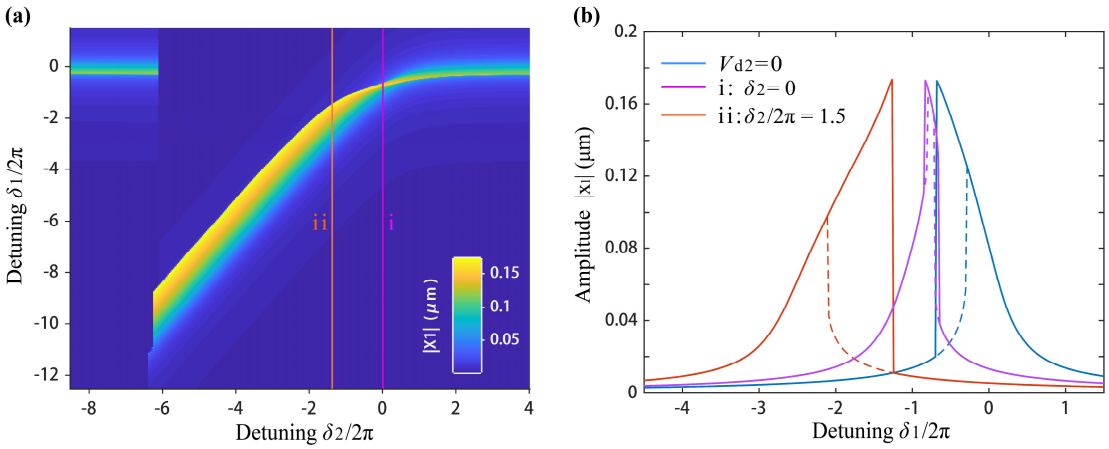

Fig.7 Simulated amplitude-frequency responses of mode 1 along with the changes of driving voltage and detuning of mode 2. (**a**) shows the amplitude-frequency responses $|x_1|$ when driving voltages V_{d1}= 4 mV and V_{d2}= 22 mV. In (**b**), the solid blue curve corresponds to the stiffness-softening bifurcation state of mode 1. Curve i is the transition point. Curve ii shows the bifurcation reversal effect of mode 1 with non-positive detuning δ_2. The dotted lines exhibit the responses with reverse sweep.

The sign transition of Duffing constant from negative to positive in Figure 7 demonstrates that by driving mode 2 with certain driving voltage and detuning, the nonlinearity of strongly driven mode 1 can be restrained and even reversed. This indicates that we can extend the input range of one mode by driving another mode on resonance at high amplitudes, which reveals the possibility of linear transduction of very large amplitudes for capacitive electromechanical resonators. Similar phenomenon was observed by applying nonlinear electrostatic field to a stiffness-hardening clamped-clamped resonator [36]. This early reported bifurcation reversal effect depends on mode index and the amount of initial tension in a nanomechanical resonator. Here, we demonstrate that the bifurcation reversal can be realized by pure coupling method, which is independent of mode index.

4. Conclusions

In this paper, we give the theoretical model for the electrostatic dispersive parametric coupling in detail. The solutions of the coupled nonlinear equations are obtained based on the multiple-time-scale analysis. By analyzing the amplitude-frequency responses of the coupled model, the dispersive parametric coupling effect is simulated. Based on this dispersive parametric coupling, a novel transduction scheme is explored. The sensitivity of this dispersive parametric transduction is given explicitly, which is only related to the design of the monitor resonator and the coupling capacitor and can be specially engineered according to the requirement of the sensitivity. This novel displacement-to-frequency transduction scheme based on the electrostatic dispersive parametric coupling is totally different from the existing counterpart that is based on the tension modulation [37,38], which can provide even more design freedoms. This electrostatic dispersive parametric transduction scheme has the potential to be used for resonant accelerometers, gyroscopes and other MEMS devices. Moreover, the strongly actuated dispersive parametric coupling reveals the ability of tuning the bifurcation topology of capacitive resonators, and a bifurcation reversal effect is predicted. Future studies can investigate more detailed mechanism and experimental observations of the bifurcation reversal caused by electrostatic-field-induced modal interaction.

Acknowledgements: This research was funded by the National Natural Science Foundation of China, grant number 51905539 and U21A20505.

Conflicts of Interest: The authors declare no conflict of interest.

Data availability: The datasets analysed during the current study are available from the corresponding author on reasonable request.

Ethical standard: The authors state that this research complies with ethical standards.

References

1. Nguyen, C.T.C. MEMS technology for timing and frequency control. *IEEE Transactions on Ultrasonics Ferroelectrics & Frequency Control* 2007, *54*, 251–270.
2. Ng, E., Yang, Y., Hong, V.A., Ahn, C.H., Heinz, D.B., Flader, I., Chen, Y., Everhart, C.L.M., Kim, B., Melamud, R., Candler, R.N., Hopcroft, M.A., Salvia, J.C., Yoneoka, S., Graham, A.B., Agarwal, M., Messana, M.W., Chen, K.L., Lee, H.K., Wang, S., Bahl, G., Qu, V., Chiang, C.F., Kenny, T.W., Partridge, A., Lutz, M., Yama, G., O'Brien, G.J. The long path from MEMS resonators to timing products. IEEE International Conference on Micro Electro Mechanical Systems, 2015, pp. 1–2.
3. Roy, S.K., Sauer, V.T.K., Westwood-Bachman, J.N., Venkatasubramanian, A., Hiebert, W.K. Improving mechanical sensor performance through larger damping. *Science* 2018, *360*, eaar5220.
4. Moser, J., Güttinger, J., Eichler, A., Esplandiu, M.J., Liu, D.E., Dykman, M.I., Bachtold, A. Ultrasensitive force detection with a nanotube mechanical resonator. *Nature Nanotechnology* 2013, *8*, 493–496.
5. Middlemiss, R.P., Samarelli, A., Paul, D.J., Hough, J., Rowan, S., Hammond, G.D. Measurement of the Earth tides with a MEMS gravimeter. *Nature* 2016, *531*, 614–617.
6. Hafifiz, M.A.A., Kosuru, L., Younis, M.I. Microelectromechanical reprogrammable logic device. *Nature Communications* 2016, *7*, 11137.

7. Hatanaka, D., Mahboob, I., Onomitsu, K., Yamaguchi, H. Phonon waveguides for electromechanical circuits. *Nature Nanotechnology* 2014, *9*, 520–524.
8. Riedinger, R., Wallucks, A., Marinkovi´c, I., Löschnauer, C., Aspelmeyer, M., Hong, S., Gröblacher, S. Remote quantum entanglement between two micromechanical oscillators. *Nature* 2018, *556*, 473–477.
9. Wollman, E.E., Lei, C.U., Weinstein, A.J., Suh, J., Kronwald, A., Marquardt, F., Clerk, A.A., Schwab, K.C. Quantum squeezing of motion in a mechanical resonator. Science 2015, 349, 952–955.
10. Zhao, C., Montaseri, M.H., Wood, G.S., Pu, S.H., Seshia, A.A., Kraft, M. A review on coupled MEMS resonators for sensing applications utilizing mode localization. Sensors and Actuators A: Physical 2016, 249, 93–111.
11. Kenig, E., Cross, M.C., Lifshitz, R., Karabalin, R.B., Villanueva, L.G., Matheny, M.H., Roukes, M.L. Passive Phase Noise Cancellation Scheme. Phys. Rev. Lett. 2012, 108, 264102. doi:10.1103/PhysRevLett.108.264102.
12. Antonio, D., Zanette, D.H., López, D. Frequency stabilization in nonlinear micromechanical oscillators. Nature Communications 2012, 3, 806.
13. Westra, H.J.R., Poot, M., van der Zant, H.S.J., Venstra, W.J. Nonlinear modal interactions in clamped-clamped mechanical resonators. Physical Review Letters 2010, 105, 117205.
14. Eichler, A., Del Álamo Ruiz, M., Plaza, J.A., Bachtold, A. Strong coupling between mechanical modes in a nanotube resonator. Physical Review Letters 2012, 109, 025503.
15. Faust, T., Rieger, J., Seitner, M.J., Krenn, P., Kotthaus, J.P., Weig, E.M. Nonadiabatic dynamics of two strongly coupled nanomechanical resonator modes. Physical Review Letters 2012, 109, 037205.
16. Matheny, M.H., Villanueva, L.G., Karabalin, R.B., Sader, J.E., Roukes, M.L. Nonlinear Mode-Coupling in Nanomechanical Systems. Nano Letters 2013, 13, 1622–1626.
17. Okamoto, H., Gourgout, A., Chang, C.Y., Onomitsu, K., Mahboob, I., Chang, E.Y., Yamaguchi, H. Coherent phonon manipulation in coupled mechanical resonators. Nature Physics 2013, 9, 598–598.
18. Mahboob, I., Perrissin, N., Nishiguchi, K., Hatanaka, D., Okazaki, Y., Fujiwara, A., Yamaguchi, H. Dispersive and dissipative coupling in a micromechanical resonator embedded with a nanomechanical resonator. Nano Letters 2015, 15, 2312–2317.
19. Zhou, X., Zhao, C., Xiao, D., Sun, J., Sobreviela, G., Gerrard, D.D., Chen, Y., Flader, I., Kenny, T.W., Wu, X., Seshia, A.A. Dynamic modulation of modal coupling in microelectromechanical gyroscopic ring resonators. Nature Communications 2019, 10, 4980.
20. Mahboob, I., Mounaix, M., Nishiguchi, K. *et al.* A multimode electromechanical parametric resonator array. *Sci Rep* 4**,** 4448 (2014).
21. Karabalin, R. B., Cross, M. C., Roukes, M. L. Nonlinear dynamics and chaos in two coupled nanomechanical resonators. PhysRevB. 79.165309 (2009).
22. Venstra, W.J., van Leeuwen, R., van der Zant, H.S.J. Strongly coupled modes in a weakly driven micromechanical resonator. Applied Physics Letters 2012, 101, 243111.
23. Mahboob, I., Nishiguchi, K., Okamoto, H., Yamaguchi, H. Phonon-cavity electromechanics. Nature Physics 2012, 8, 387–392.
24. Li, L., Zhang, Q., Wang, W. *et al.* Nonlinear coupled vibration of electrostatically actuated clamped–clamped microbeams under higher-order modes excitation. *Nonlinear Dyn* **90,** 1593–1606 (2017).
25. Lu, K., Li, Q., Zhou, X., Song, G., Wu, K., D. Modal Coupling Effect in a Novel NonlinearMicromechanical Resonator. Micromachines 2020,11. doi:10.3390/mi 1105 0472.
26. Lu, K., Zhou, X., Li, Q., Wu, K., Zhang, Y., Zhuo, M., Wu, X., Xiao, D. A Wide Range Frequency Coherent Modulation Control Based on Modal Coupling Effect in MEMS Resonators. 2021

IEEE 34th International Conference on Micro Electro Mechanical Systems (MEMS), 2021, pp. 161–164. doi:10.1109/MEMS51782.2021.9375233.
27. Agrawal, D.K., Woodhouse, J., Seshia, A.A. Observation of locked phase dynamics and enhanced frequency stability in synchronized micromechanical oscillators. Physical Review Letters 2013, 111, 084101.
28. Husain., A., Hone., J., Ch.., Postma., Henk., W., Huang., X., M.H. Nanowire-based very-high-frequency electromechanical resonator. Applied Physics Letters 2003, 83, 1240–1240.
29. Sazonova, V., Yaish, Y., Ustunel, H., Roundy, D., Arias, T.A., Mceuen, P.L. A tunable carbon nanotube electromechanical oscillator. Nature 2012, 431, 284–7.
30. Wen, Y., Ares, N., Schupp, F.J., Pei, T., Laird, E.A. A coherent nanomechanical oscillator driven by single-electron tunnelling. Nature Physics 2020, 16, 1–8.
31. Lifshitz, R., Cross, M.C. Nonlinear Dynamics of Nanomechanical and Micromechanical Resonators, Wiley-VCH Verlag GmbH & Co. KGaA, 2008, pp. 1–52.
32. Nayfeh, A.H., Mook, D.T. Nonlinear Oscillations, Wiley-VCH Verlag GmbH & Co. KGaA, 1995.
33. Kambali, P.N., Pandey, A.K. Nonlinear coupling of transverse modes of a fixed–fixed microbeam under direct and parametric excitation. *Nonlinear Dyn* **87,** 1271–1294 (2017).
34. Daeichin, M., Miles, R. & Towfighian, S. Lateral pull-in instability of electrostatic MEMS transducers employing repulsive force. *Nonlinear Dyn* **100,** 1927–1940 (2020).
35. Holmes, P.J., Rand, D.A. The bifurcations of duffing's equation: An application of catastrophe theory. Journal of Sound & Vibration 1976, 44, 237–253.
36. Khan, Raphaël., Massel, F., Heikkilä, T. T. Tension-induced nonlinearities of flexural modes in nanomechanical resonators. Physical Review B 2013, 87, 235406.
37. Zou, X., Thiruvenkatanathan, P., Seshia, A.A. A Seismic-Grade Resonant MEMS Accelerometer. Journal of Microelectromechanical Systems 2014, 23, 768–770.
38. Mustafazade, A., Pandit, M., Zhao, C., Sobreviela, G., Du, Z., Steinmann, P., Zou, X., Howe, R.T., Seshia, A.A. A vibrating beam MEMS accelerometer for gravity and seismic measurements. Scientifific Reports 2020, 10, 10415.